ACS OMEGA

http://pubs.acs.org/journal/acsodf

Article

Anionic-Surfactant-Stabilized Hydrophobic Ionic-Liquid-Based Bicontinuous Microemulsion as a Medium for Enzymatic Oxidative Polymerization of Aniline

Rongrong Wang and Xirong Huang*

Cite This: *ACS Omega* 2021, 6, 20699−20709

Read Online

ACCESS | Metrics & More | Article Recommendations | Supporting Information

ABSTRACT: The hydrophobic ionic liquid [C_8mim][PF_6] (1-octyl-3-methylimidazolium hexafluorophosphate)-based bicontinuous microemulsion stabilized by the anionic surfactant [C_4mim][AOT] (1-butyl-3-methylimidazolium bis(2-ethylhexyl) sulfosuccinate) was first tried as a medium for horseradish peroxidase (HRP)-triggered oxidative polymerization of aniline. The effects of the mass ratio of [C_8mim][PF_6]-to-water (α), the mass fraction of [C_4mim][AOT] in the total mixture (γ), and temperature (T) on the enzymatic polymerization were investigated using UV−vis−NIR absorption, electron spin resonance, and small-angle X-ray scattering spectroscopy techniques. The bicontinuous microemulsion is demonstrated to play a template role in the biosynthesis of polyaniline (PANI). The conductivity of the resulting PANI depends on the microemulsion microstructure and the microstructure- and T-dependent catalytic properties of the solubilized HRP. With the increase in α, the conductivity of the synthesized PANI decreases due to the increase in the template curvature (decrease of the microdomain size) and the decrease in the activity and stability of HRP. Compared with α, γ has little effect on the microdomain size of the template; so, the γ-dependent change in the conductivity of PANI is mainly caused by the changes of the microstructure-dependent activity and stability of HRP. Over the range of 20−35 °C, T has little effect on the microdomain size, but it greatly changes the activity and stability of HRP. With the increase in T, the activity of HRP increases steadily, but its stability decreases significantly, which should be one of the reasons why the conductivity of PANI decreases with increasing T. In conclusion, lower values of α, γ, and T are favorable for the biosynthesis of conductive PANI. The present study not only deepens the insight into the role of the template in the process of PANI synthesis, but also opens up a green new way for the biosynthesis of the conducting polymer.

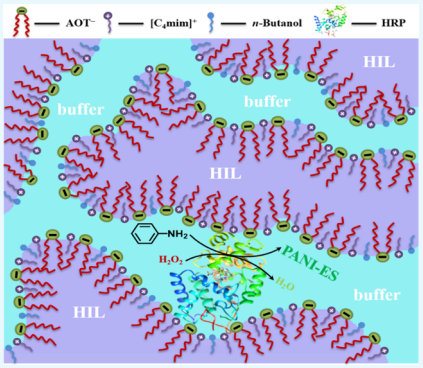

INTRODUCTION

Conducting polymers are a very important kind of polymer material, and they have wide applications in the fields of electromagnetic shielding, energy storage, electrochromic display devices, sensors, and so on. As one of the most promising conducting polymers, polyaniline (PANI) has been extensively studied.[1−5] Usually, PANI is synthesized chemically or electrochemically.[6−8] These traditional polymerization methods usually need harsh reaction conditions, resulting in an adverse effect on the environment. Relatively speaking, the biosynthesis of PANI is an environmentally benign strategy, and this strategy has attracted great attention in recent decades.[9−11]

So far, there have been many attempts to synthesize PANI by oxidoreductase-catalyzed oxidative polymerization.[11−17] In addition to the biocatalyst, templates are also found to be a key parameter for the biosynthesis of PANI. It is believed that the templates can interact directly with the reacting aniline monomer and the growing polymer chains, or they can spatially confine the reaction to reduce the occurrence of side reactions, and finally control the chemical structure and morphology of the synthesized PANI.[13,18,19] The templates used for the enzymatic polymerization of aniline are mostly soft templates, which are composed of strong acid-type polyelectrolytes or strong acid-type surfactant aggregates. Compared with polyanionic templates, the surfactant aggregates as templates are more favorable due to their well-defined microstructure and multiple microstructure-tuning parameters. Many reports have been released on the use of the anionic surfactant, especially bis(2-ethylhexyl)sulfosuccinate (AOT)-based micelles[20−25] and vesicles[26−29] as templates for the biosynthesis of conductive PANI. However, less attempt has been made to utilize the anionic surfactant-stabilized microemulsions, especially bicontinuous microemulsions as templates.[30] Compared with droplet-type microemulsions, bicon-

Received: June 16, 2021
Accepted: July 19, 2021
Published: July 28, 2021

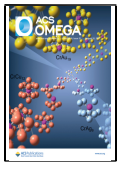

https://doi.org/10.1021/acsomega.1c03150
ACS Omega 2021, 6, 20699−20709

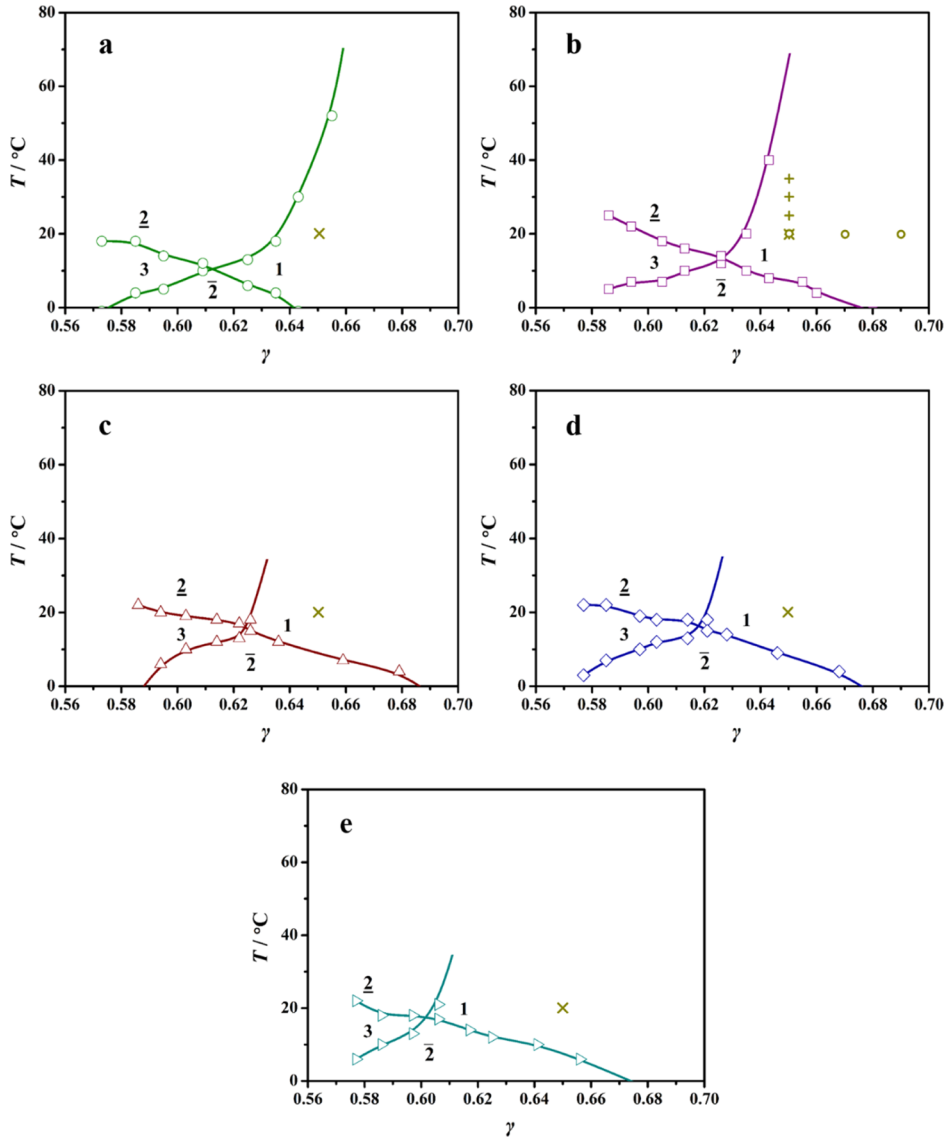

Figure 1. Effect of α on the fishlike phase diagram (fish-tail part) of the [C_8mim][PF_6]/buffer/[C_4mim][AOT]/*n*-butanol (δ = 0.100) pseudoternary system [α = 0.250 (a), 0.350 (b), 0.450 (c), 0.500 (d), and 0.552 (e)]. The signs (×, +, and ○) in the fish-tail region are the sampling points for the preparation of the microemulsion as a medium for the subsequent polymerization reaction. The symbols of 2̄, 3, 1, and 2 represent Winsor I-type microemulsion (i.e., upper-phase HIL/W-type microemulsion coexisting with a HIL excess phase), Winsor III-type microemulsion (i.e., middle-phase microemulsion coexisting with both a HIL excess phase and a water excess phase), Winsor IV-type bicontinuous microemulsion, and Winsor II-type microemulsion (i.e., lower-phase W/HIL-type microemulsion coexisting with a water excess phase), respectively.

tinuous microemulsions have some unique properties, such as high solubilization capacity, large interfacial area, and zero-averaged interfacial curvature.[31−34] The utilization of anionic surfactant-stabilized bicontinuous microemulsions as templates for the enzymatic polymerization of aniline may be more conducive to controlling the morphology of PANI and resulting in high-quality PANI. A first attempt has been made by our group, and the study on the enzymatic polymerization of aniline in the traditional bicontinuous microemulsion medium indicates that the bicontinuous microemulsion can act as a template in the biosynthesis of PANI, and the conductivity of the synthesized PANI depends on the template microstructure as well as the activity and stability of the solubilized enzyme.[35,36]

An ionic liquid (IL) is a molten organic salt composed of an organic cation and an organic or inorganic anion with a melting point at room temperature or below 100 °C. Compared with molecular solvents, ILs could be regarded as "green solvents" due to their low saturated vapor pressure.[37] The use of hydrophobic ionic liquid (HIL) instead of a traditional molecular organic solvent as an oil phase to construct a green bicontinuous microemulsion has recently attracted great attention. At present, some HIL-based bicontinuous microemulsions stabilized by nonionic surfactants are available,[38−42] but their phase inversion temperatures are mostly high, resulting in their incompatibility with enzymes. In view of the template effect of anionic surfactant aggregates in the biosynthesis of PANI, it is significant to construct an anionic surfactant-stabilized HIL-based bicontinuous microemulsion with moderate phase inversion temperature. Till now, there has been no report on the biosynthesis of conductive PANI in a green microemulsion medium. The

https://doi.org/10.1021/acsomega.1c03150
ACS Omega 2021, 6, 20699−20709

present study will open up a green new way for the biosynthesis of conductive PANI.

RESULTS AND DISCUSSION

Effect of the Mass Ratio of HIL-to-Water (α) on the Enzymatic Polymerization of Aniline. The anionic surfactant bis(2-ethylhexyl) sulfosuccinate sodium salt (NaAOT), which is commercially available, is commonly used to construct self-organized systems as anionic templates for enzymatic polymerization of aniline.[15,22,35] As NaAOT is scarcely soluble in HIL, a surfactant counterion replacement strategy was adopted in our previous work to enhance its solubility in HIL. Using this strategy, we successfully constructed an AOT-stabilized HIL-based bicontinuous microemulsion.[43,44] Based on our previous study on the influence of the alkyl-chain length (n) on the cation $[C_n mim]^+$ (1-alkyl-3-methylimidazolium) on the phase behavior of the water (buffer)/$[C_n mim][AOT]$/$[C_n mim][PF_6]$ microemulsion, here, $[C_4 mim][AOT]$ and $[C_8 mim][PF_6]$ are selected as the surfactant and the oil phase, respectively. In order to be able to select appropriate composition for the microemulsion as the medium for enzymatic oxidative polymerization of aniline, it is necessary to draw the $T-\gamma$ fishlike phase diagram (fish-tail part) of the $[C_4 mim][AOT]$/$[C_8 mim][PF_6]$/buffer (50 mM NaH_2PO_4, pH = 4.3)/n-butanol pseudoternary system (δ = 0.100) at different α values (γ, δ, and α are defined as the mass fractions of the surfactant (with alcohol) in the total mixture, the alcohol in the mixture of the surfactant and alcohol, and the HIL in the mixture of the HIL and buffer, respectively). The corresponding results are shown in Figure 1 and Table 1.

Table 1. Characteristic Parameters of the Fishlike Phase Diagrams (Fish-Tail Part) of the Pseudoternary System at Different α Values[a]

α	$\tilde{\gamma}$	$\tilde{T}$/°C
0.250	0.612	10
0.350	0.626	13
0.450	0.626	16
0.500	0.621	17
0.552	0.606	19

[a] $\tilde{\gamma}$ is the lowest surfactant concentration (i.e., the surfactant efficiency) beyond which the Winsor IV phase is formed, and $\tilde{T}$ is the corresponding phase inversion temperature.

Over the α range studied, the $[C_4 mim][AOT]$-stabilized $[C_8 mim][PF_6]$-based microemulsion systems display moderate phase inversion temperatures, indicating that these systems could be used as media for the biosynthesis of PANI. Just as in the traditional oil/water system,[45,46] here, the coordinates of the fish-tail points vary with the change in the α value. Table 1 shows that as α increases, the surfactant efficiency $\tilde{\gamma}$ changes little, but the phase inversion temperature $\tilde{T}$ increases. This changing trend goes contrary to that observed in the traditional oil/water system stabilized by the ionic surfactant NaAOT, in which $\tilde{T}$ decreases with the increase in α.[46,47] This is mainly due to the fact that the T-dependent aggregation mechanism of the present system is different from that of a classic water/NaAOT/oil system, although both systems have the same T-dependent apparent phase sequence.[43]

Figure 2 shows the UV−vis−NIR absorption spectra of the reaction systems which were recorded after 12 h horseradish peroxidase (HRP)-catalyzed polymerization of aniline in different bicontinuous microemulsions (varying α at constant T and γ, the composition of the corresponding medium is identified by a "×" point in the phase diagrams shown in Figure 1). According to the literature, the absorption peaks at ca. 420 nm and ca. 1010 nm in the spectra are assigned to the characteristic absorption of conductive PANI (especially the peak at ca. 1010 nm, its intensity is positively correlated with the conductivity of the resulting PANI).[28,48] The absorption at ca. 565 nm could be ascribed to the branching of the resulting PANI[20] or the formation of phenazine units during the reaction.[49] It can be seen from Figure 2 that with the decrease of α, the intensity of the characteristic absorption peaks of the resulting PANI increases significantly, and moreover, the peak in the NIR region red-shifts (from 987 to 1015 nm), indicating that smaller α favors the linear growth of PANI, and the resulting PANI is more conductive.[6,30]

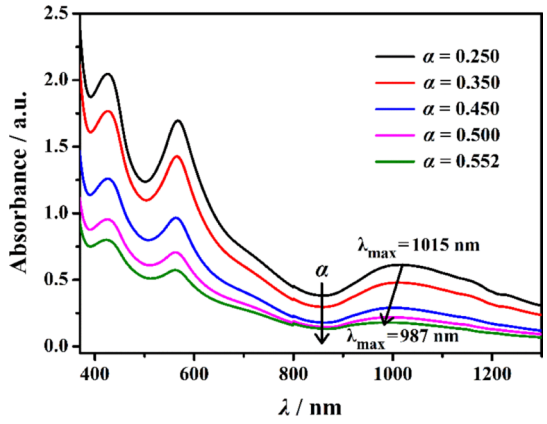

Figure 2. UV−vis−NIR absorption spectra of the reaction systems (δ = 0.100, γ = 0.650, and $T_{reaction}$ = 20 °C) at different α values (the α value gradually increases from top to bottom) after 12 h HRP-catalyzed polymerization of aniline ($[aniline]_{overall}$ = 8.0 mM, $[HRP]_{overall}$ = 2.0 μM, and $[H_2O_2]_{overall}$ = 9.0 mM).

In order to confirm the above inference, the polaron concentrations of the resulting PANI systems mentioned above were measured using the electron spin resonance (ESR) technique. Figure 3 shows the corresponding ESR spectra. The derived characteristic parameters are listed in Table 2. With the increase in α, the concentration of polarons in the resulting system decreases gradually, indicating that the conductivity of

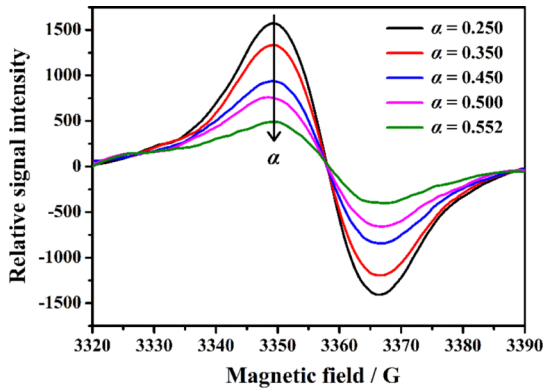

Figure 3. ESR spectra of the resulting systems after 12 h enzymatic polymerization of aniline in different bicontinuous microemulsions (with different α values). The medium and reaction conditions are the same as those in Figure 2.

https://doi.org/10.1021/acsomega.1c03150
ACS Omega 2021, 6, 20699−20709

Table 2. Corresponding Characteristic Parameters Derived from the ESR Spectra at Different α Values

α	g	ΔH_{pp}/G	spins/μM
0.250	2.003	16.44	26.23
0.350	2.003	17.07	24.22
0.450	2.003	17.62	17.39
0.500	2.003	18.56	16.35
0.552	2.003	18.77	14.47

the synthesized PANI does decrease with the increase in α. Table 2 also shows that the peak-to-peak width ΔH_{pp} gradually increases with α, indicating that the degree of delocalization of polarons in PANI decreases gradually,[48] that is, the conductivity of PANI becomes worse.

To explore the mechanism of the α effect on the conductivity of the synthesized PANI, the α-dependent microstructure of the HIL-based bicontinuous microemulsion and the effect of the microstructure on the activity and stability of the solubilized HRP were studied. The microstructure of bicontinuous microemulsions of different α values at constant T and γ values was characterized by small-angle X-ray scattering (SAXS). As can be seen from Figure 4, the scattering

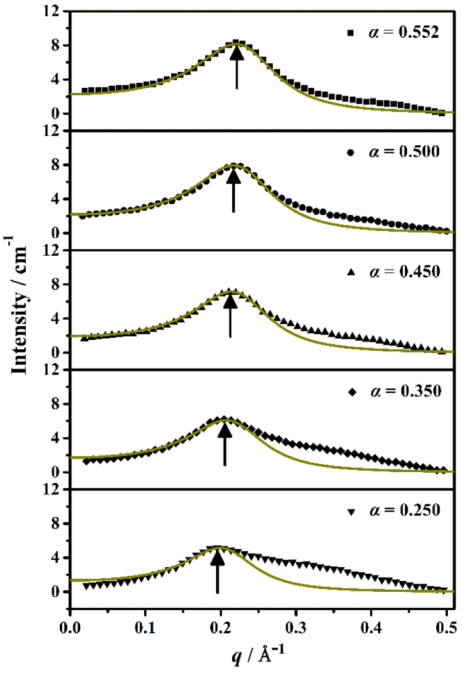

Figure 4. SAXS spectra of the $[C_8mim][PF_6]$/buffer/$[C_4mim]$-[AOT]/*n*-butanol (T = 20 °C, δ = 0.100, γ = 0.650) pseudoternary system at different α values. The samples are identified by a "×" point in Figure 1. Symbols are the experimental data, and solid lines are the T−S fits.

curves [the absolute scattering intensity $I(q)$ vs the scattering vector q] obtained at different α values are similar, and with the increase in α, the broad scattering peak shifts gradually to the right, that is, the q_{max} value becomes larger. The shoulder on the right side of the scattering curve originates from the substructure of pure IL.[50−52] *Via* the Teubner−Strey (T−S) model fitting,[53] the parameters d, ξ, and f_a of the microstructure formed by the surfactant aggregates were obtained and are summarized in Table 3, where d is the mean repeat distance of the HIL and water domains, ξ is the correlation length, and f_a is the amphiphilicity factor.

Table 3. Corresponding Microstructural Parameters of the Bicontinuous Microemulsions at Different α Values

α	d (Å)	ξ (Å)	f_a
0.250	31.5	18.2	−0.859
0.350	29.4	16.7	−0.855
0.450	28.2	15.9	−0.853
0.500	27.8	15.5	−0.850
0.552	27.4	15.1	−0.847

As shown in Table 3, within the α range studied, all f_a values are less than −0.80, indicating that all bicontinuous microemulsions have an ordered microstructure.[54] With the increase in α, both the mean repeat distance (d) and the correlation length (ξ) decrease, indicating that the corresponding microdomain size becomes smaller with the increase in the HIL content. Compared with the traditional oil/water system, the smaller d value of the present system is due to the higher surfactant content required to form the optimal single-phase microemulsion (i.e., lower surfactant efficiency), which results in a larger interfacial area and smaller HIL- and water-domain size.[55,56]

The activity and stability of the solubilized HRP in the above bicontinuous microemulsions were also measured to investigate the effect of the microstructure on HRP. Based on the kinetic curves in different microemulsions (Figure S1), the kinetic parameters of HRP in the corresponding medium were derived. Table 4 shows that the turnover number (k_{cat}) varies

Table 4. Kinetic Parameters of HRP in Bicontinuous Microemulsions of Different α Values

α	k_{cat} (s^{-1})	K_m (mM)	kcat/K_m (mM^{-1} s^{-1})
0.250	240.0	1.47	163.3
0.350	150.5	1.71	88.0
0.450	95.1	1.97	48.3
0.500	59.8	2.22	26.9
0.552	33.0	2.54	13.0

markedly with α; however, the Michaelis constant (K_m) changes little with α (a slight increase). This phenomenon could be explained as follows: as the water-domain size of the HIL-based bicontinuous microemulsion is much smaller than the molecular size of HRP,[57] the electrostatic interaction between the solubilized HRP (in the water-domain, with net positive charges at pH 4.3) and the negatively charged surfactant interface enhances gradually with the decrease in d, thereby resulting in a decrease in k_{cat}; on the other hand, the decrease of d with α at a fixed γ value makes the arrangement of the surfactant on the interface loose, and some HILs may penetrate into the surfactant palisade layer, which may have a certain impact on the HRP conformation, thereby leading to a decrease in k_{cat}.[58] The same reason can be used to explain why the stability of HRP decreases with the increase in α (as shown in Figure 5).

When the microstructure of the microemulsion and the catalytic performance of the solubilized HRP are correlated with the aforementioned α effect on the UV−vis−NIR and ESR spectra of the synthesized PANI, it is found that the conductivity of the synthesized PANI is determined by the

https://doi.org/10.1021/acsomega.1c03150
ACS Omega 2021, 6, 20699−20709

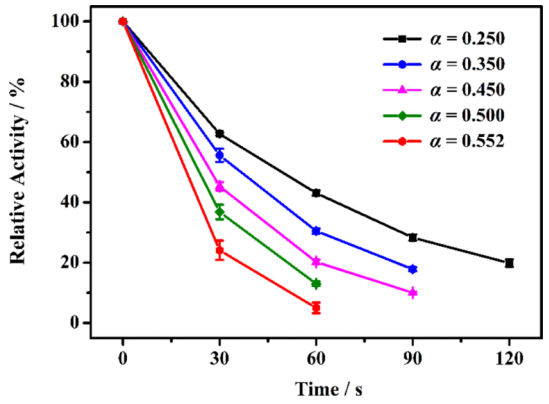

Figure 5. Effect of α on the stability of HRP in $[C_4mim][AOT]$-stabilized $[C_8mim][PF_6]$-based bicontinuous microemulsion (T = 20 °C, δ = 0.100, and γ = 0.650). ($[ABTS]_{overall}$ = 3.0 mM, $[HRP]_{overall}$ = 2.5 nM, and $[H_2O_2]_{overall}$ = 2.0 mM).

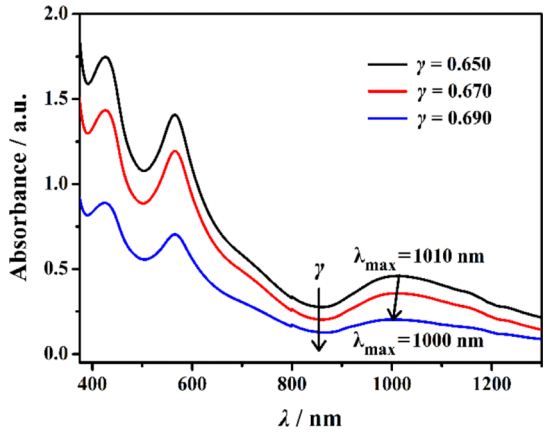

Figure 6. UV−vis−NIR absorption spectra of the resulting PANI systems of different surfactant concentrations which were sampled after 12 h enzymatic polymerization of aniline in bicontinuous microemulsions (α = 0.350, δ = 0.100, $[aniline]_{overall}$ = 8.0 mM, $[HRP]_{overall}$ = 2.0 μM, $[H_2O_2]_{overall}$ = 9.0 mM, and $T_{reaction}$ = 20 °C).

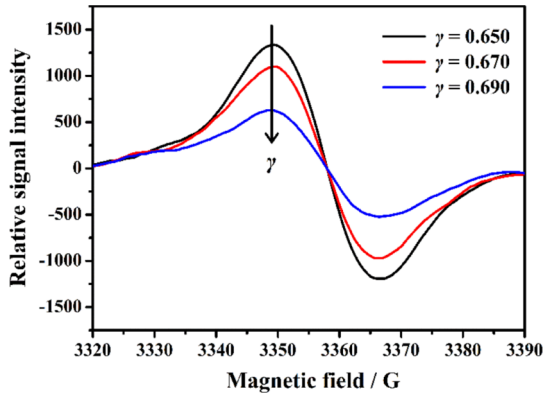

Figure 7. ESR spectra of the resulting PANI systems sampled after 12 h enzymatic polymerization of aniline in bicontinuous microemulsions of different γ values. The medium and reaction conditions are identical to those shown in the caption of Figure 6.

microstructure of the bicontinuous microemulsion and the microstructure-dependent enzymatic properties of the solubilized HRP. As α increases, the microdomain size d decreases and the interfacial curvature of the microdomain increases, which may be unfavorable to the linear growth of PANI, thus leading to a blue shift of the absorption peak in the NIR region and a decrease in the polaron concentration of the PANI system. In addition, the decrease in the activity and stability of HRP with increasing α reduces the amount of the synthesized PANI, which makes the characteristic absorption and the polaron concentration of the polymerization system decrease.[35,36] It follows that the bicontinuous microemulsion has a microenvironmental effect on the solubilized HRP and a template effect on the HRP-catalyzed polymerization of aniline.

Effect of the Surfactant Concentration (γ) on the Enzymatic Polymerization of Aniline. In a traditional microemulsion system, the surfactant content is one of the important factors affecting the microstructure of the microemulsion.[53,55,56] Therefore, the γ effect on the HRP-catalyzed polymerization of aniline in the present bicontinuous microemulsion system was explored (the microemulsion composition is identified by a "○" point in Figure 1). It can be seen from Figure 6 that with the increase in γ, the intensity of the absorption peak in the NIR region decreases, and the decrease is accompanied by a small blue shift (from 1010 to 1000 nm). The above result indicates that the conductivity of the synthesized PANI decreases with the increase in γ. This inference is supported by the ESR results (Figure 7 and Table 5). It is shown that with the increase in γ, the polaron concentration in the PANI system decreases gradually and the ΔH_{pp} increases a little, confirming that the conductivity of the synthesized PANI decreases with the increase in γ.

To explore the mechanism of the γ effect on the conductivity of the synthesized PANI, the microstructure of the HIL-based bicontinuous microemulsion and the catalytic performance of the solubilized HRP at different γ values were investigated. Figure 8 shows the SAXS data of bicontinuous microemulsion systems at different γ values at 20 °C. The corresponding microstructural parameters obtained by T−S model fitting are listed in Table 6. Table 6 indicates that as γ increases, d decreases slightly, but ξ remains unchanged. This trend is quite different from that observed in a traditional oil/water system in which the d and ξ values decrease markedly with increasing γ.[53] This difference should be ascribed to the low surfactant efficiency of the present HIL/water system.[55]

Table 5. Corresponding Characteristic Parameters of ESR Spectra Recorded in Figure 7

γ	g	ΔH_{pp}/G	spins/μM
0.650	2.003	17.07	24.22
0.670	2.003	17.22	16.51
0.690	2.003	18.60	14.96

The kinetics of the solubilized HRP was also studied to understand the microenvironmental effect of the medium on HRP in the bicontinuous microemulsions of different γ values (see Figure S2). As can be seen from Table 7, with the increase in γ, k_{cat} decreases markedly, while K_m increases slightly. As a result, the catalytic efficiency (k_{cat}/K_m) decreases significantly with increasing γ. This is mainly caused by the high surfactant concentration. The high surfactant concentration results in a small water domain size, and the small water domain size can significantly enhance the electrostatic interaction between HRP and the surfactant. Although the dependence of d on γ at high surfactant concentration is no longer significant, the electrostatic interaction becomes stronger, so k_{cat} is decreased

https://doi.org/10.1021/acsomega.1c03150
ACS Omega 2021, 6, 20699−20709

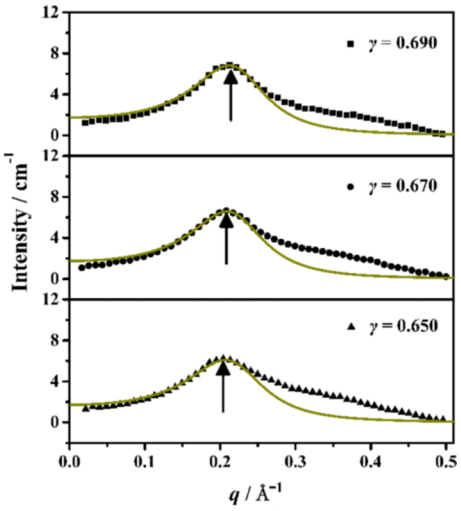

Figure 8. SAXS spectra of different bicontinuous microemulsion systems at 20 °C. (α = 0.350; δ = 0.100; and γ = 0.650, 0.670, or 0.690). The samples are identified by a "○" point in Figure 1. Symbols are the experimental data, and solid lines are the T−S fits.

Table 6. Corresponding Microstructural Parameters of Bicontinuous Microemulsion Systems at Different γ Values Derived from Figure 8

γ	d (Å)	ξ (Å)	f_a
0.650	29.4	16.7	−0.855
0.670	28.9	16.5	−0.857
0.690	28.5	16.7	−0.862

Table 7. Kinetic Parameters of HRP in Different Bicontinuous Microemulsions

γ	k_{cat} (s−1)	K_m (mM)	kcat/K_m (mM^{-1} s^{-1})
0.650	150.5	1.71	88.0
0.670	108.1	1.90	56.9
0.690	52.8	2.30	23.0

significantly with the increase in γ.[44] This is also the reason why the stability of HRP decreases with the increase in γ (Figure 9).

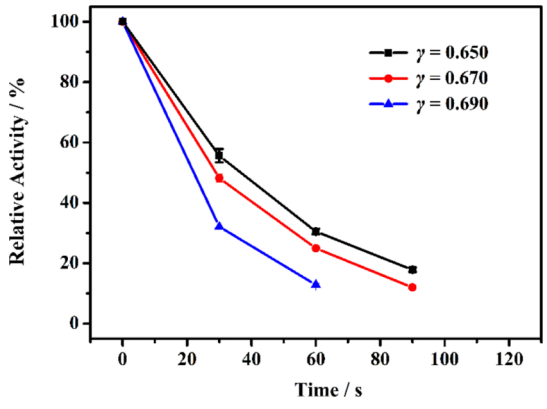

Figure 9. Effect of γ on the stability of HRP in [C_4mim][AOT]-stabilized [C_8mim][PF_6]-based bicontinuous microemulsion medium (T = 20 °C, α = 0.350, and δ = 0.100). ($[ABTS]_{overall}$ = 3.0 mM, $[HRP]_{overall}$ = 2.5 nM, and $[H_2O_2]_{overall}$ = 2.0 mM).

Based on the γ-dependent microstructure of the HIL-based bicontinuous microemulsion and the microstructure-dependent catalytic performance of the solubilized HRP in the system, together with the γ effect on the UV−vis−NIR characteristic absorption and the polaron concentration of the PANI synthesis system, the following inference could be drawn. The present γ effect is caused mainly by the microstructure-dependent catalytic performance of HRP. The reasons are as follows. With the increase in γ, the microdomain size of the HIL-based bicontinuous microemulsion changes little, and the blue shift of the characteristic absorption peak in the NIR region is also small, so the template effect of the microstructure should not be responsible for the significant change of the conductivity of PANI with γ. However, the catalytic activity and stability of the solubilized HRP decrease significantly with the increase in γ, which reduces the amount of PANI synthesized in the system, thus leading to a decrease in the conductivity of the PANI synthesis system.

Effect of Temperature (T) on the Enzymatic Polymerization of Aniline. The HRP-catalyzed polymerization of aniline in the HIL-based bicontinuous microemulsion was studied at different temperatures to understand the temperature effect. Figure 10 shows the UV−vis−NIR absorption spectra of the resulting PANI synthesis systems sampled after 12 h reaction in the bicontinuous microemulsion (the composition of the microemulsion is identified by a "+" point in the phase diagrams shown in Figure 1). It can be seen from Figure 10 that the characteristic absorption peaks of the PANI synthesis system are varied with T. Specifically, with the increase in T, the absorption at 1000 nm (A_{1000nm}) decreases significantly, while the absorption at 565 nm (A_{565nm}) increases gradually, and the ratio of A_{1000nm} to A_{565nm} decreases accordingly with the increase in T (see Figure 10B). In addition, the absorption peak in the NIR region blue-shifts significantly (from 1010 to 983 nm) with increasing T. The above results indicate that the higher the T value, the worse the linear growth of PANI, and thus the poorer the conductivity of the synthesized PANI. This inference is corroborated by the ESR results (see Figure 11 and Table 8). As T increases, the polaron concentration in the system decreases gradually, and the ΔH_{pp} increases a little, demonstrating that the conductivity of the synthesized PANI decreases with the increase in T.

In order to explore the mechanism of the T effect on the conductivity of the synthesized PANI, the microstructure of HIL-based bicontinuous microemulsion and the catalytic performance of the solubilized HRP at different temperatures were also studied. Figure 12 shows the $I(q) \sim q$ curves of the bicontinuous microemulsion systems (α = 0.350, γ = 0.650, and δ = 0.100) at different temperatures. The microstructural parameters of the corresponding microemulsion system were obtained via T−S model fitting (Table 9). Interestingly, temperature has little effect on the microdomain size of the bicontinuous microemulsion over the T range studied.

Now that the microdomain size of the microemulsion changes little with T, the indirect effect of T on the HRP activity caused by the microstructure can be neglected. In other words, the activity of HRP can be directly used to study the direct effect of T on HRP. The activity and stability of the solubilized HRP at different temperatures are shown in Figure 13. The T-dependent activity of HRP in the bicontinuous microemulsion indicates that there exists an optimal temperature (about 35 °C) for HRP (Figure 13A); the stability of the

https://doi.org/10.1021/acsomega.1c03150
ACS Omega 2021, 6, 20699−20709

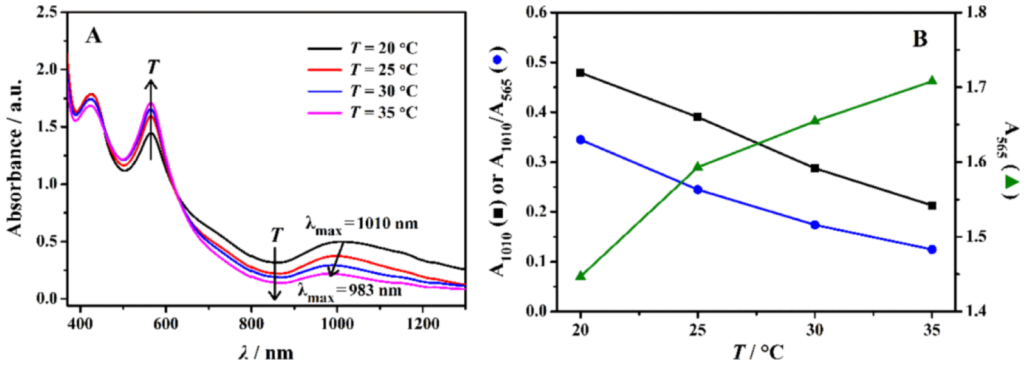

Figure 10. (A) UV−vis−NIR absorption spectra of the resulting systems at different T_s after 12 h HRP-catalyzed polymerization of aniline in the [C_4mim][AOT]-stabilized [C_8mim][PF_6]-based bicontinuous microemulsion (α = 0.350, γ = 0.650, and δ = 0.100). (B) Changes of A_{1010}, A_{565}, and A_{1010}/A_{565} with T. ([Aniline]$_{overall}$ = 8.0 mM, [HRP]$_{overall}$ = 2.0 μM, and [H_2O_2]$_{overall}$ = 9.0 mM).

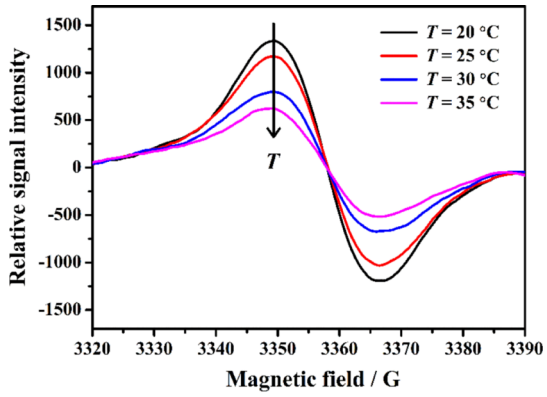

Figure 11. Effect of T on the ESR spectra of the resulting system after 12 h enzymatic polymerization of aniline in bicontinuous microemulsions (α = 0.350, γ = 0.650, and δ = 0.100) ([aniline]$_{overall}$ = 8.0 mM, [HRP]$_{overall}$ = 2.0 μM, and [H_2O_2]$_{overall}$ = 9.0 mM).

Table 8. Characteristic Parameters Derived from the ESR Spectra Shown in Figure 11

T	g	ΔH_{pp}/G	spins/μM
20	2.003	17.07	24.22
25	2.003	17.13	21.59
30	2.003	17.90	16.85
35	2.003	18.18	15.46

solubilized HRP, however, always decreases markedly with an increase in T (Figure 13B).

Based on the T effect on the microstructure of the microemulsion and the activity and stability of the solubilized HRP, together with the T effect on the UV−vis−NIR characteristic absorption and the polaron concentration of the synthesized PANI system, it can be inferred that it is the stability of HRP, not the template effect of the microstructure of the microemulsion, that should be responsible for the change of the conductivity of the synthesized PANI with T. The fact that the microdomain size of the HIL-based bicontinuous microemulsion changes little with T but the stability of HRP decreases markedly with the increase in T supports this inference.[35] It is known that the oxidative polymerization of aniline is a free-radical reaction, and higher reaction temperature may result in a higher degree of branching whether or not the enzyme is involved in the polymerization.[59,60] Hence, a relatively low temperature is conducive to the biosynthesis of high-quality PANI in the green [C_4mim][AOT]-stabilized [C_8mim][PF_6]-based bicontinuous microemulsion system.

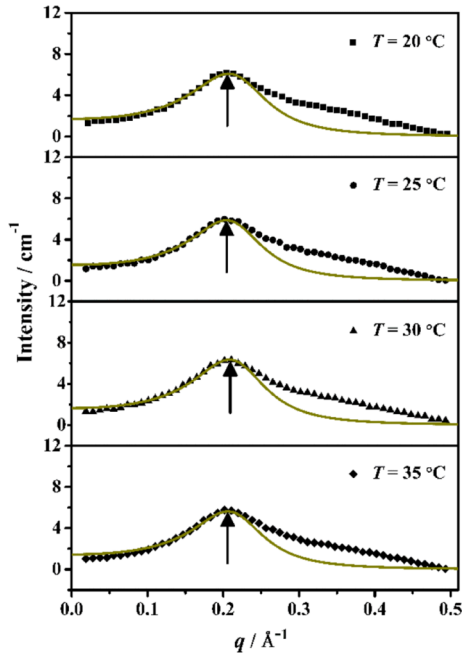

Figure 12. SAXS curves of the [C_4mim][AOT]-stabilized [C_8mim]-[PF_6]-based bicontinuous microemulsions at different T_s (α = 0.350, γ = 0.650, and δ = 0.100). The samples are identified by a "+" point in Figure 1. Symbols are the experimental data, and solid lines are the T−S fits.

Table 9. Corresponding Microstructural Parameters of the above Pseudoternary Systems at Different T_s

T (°C)	d (Å)	ξ (Å)	f_a
20	29.4	16.7	−0.855
25	29.5	17.0	−0.858
30	29.2	17.0	−0.861
35	29.3	17.1	−0.862

CONCLUSIONS

In the present work, the effects of the composition of the HIL-based microemulsion and T on the enzymatic polymerization of aniline were explored for the first time. The study demonstrates that the [C_4mim][AOT]-stabilized [C_8mim]-[PF_6]-based bicontinuous microemulsion takes a template role

https://doi.org/10.1021/acsomega.1c03150
ACS Omega 2021, 6, 20699−20709

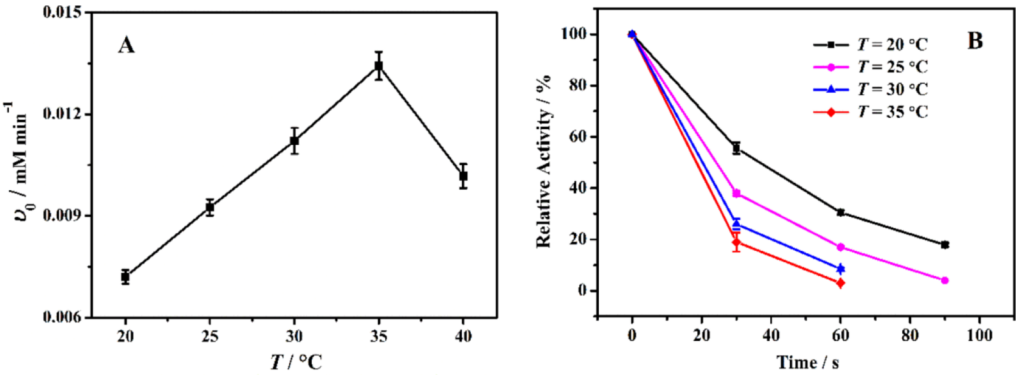

Figure 13. Activity ($[HRP]_{overall}$ = 1.0 nM) (A) and stability ($[HRP]_{overall}$ = 2.5 nM) (B) of the solubilized HRP in the bicontinuous microemulsions at different T_s (α = 0.350, γ = 0.650, and δ = 0.100). ($[ABTS]_{overall}$ = 3.0 mM and $[H_2O_2]_{overall}$ = 2.0 mM).

in the biosynthesis of PANI, and the conductivity of the synthesized PANI depends on the microemulsion microstructure and the microstructure- and T-dependent catalytic performance of the solubilized HRP. The conductivity of the synthesized PANI decreases with the increase in α due to the increase in the template curvature (decrease of the microdomain size) and the decrease in the activity and stability of HRP. Compared with α, γ has little effect on the microdomain size of the template; so, the γ-dependent change of the conductivity of the synthesized PANI is mainly caused by the changes in the microenvironment-dependent activity and stability of HRP. For T, it is found that over the range of 20−35 °C, T has little effect on the microdomain size. With the increase in T, the activity of HRP increases steadily, but its stability decreases significantly, which should be responsible for the decrease in the PANI conductivity with increasing T. Within the scope of the study, lower values of α, γ, and T (i.e., α = 0.250, γ = 0.650, and T = 20 °C) are conducive to the biosynthesis of conductive PANI. The present studies open up a green new way for the biosynthesis of conductive PANI.

EXPERIMENTAL SECTION

Materials. NaAOT (≥97%) and 2,2′-azino-bis(3-ethylbenzothiazoline-6-sulfonic acid) diammonium salt (ABTS, ≥98%) were obtained from Sigma-Aldrich. HRP (powder, EC 1.11.1.7) was purchased from Aladdin Co., Ltd. 1-Butyl-3-methylimidazolium chloride ([C_4mim][Cl], >98%) and 1-octyl-3-methylimidazolium hexafluorophosphate ([C_8mim][PF_6], >98%) were purchased from TCI Co., Ltd. 2,2-Diphenyl-1-picrylhydrazyl (DPPH, ≥98.5%) was obtained from Shanghai Macklin Biochemical Technology Co., Ltd. n-Butanol (n-C_4H_9OH, AR), sodium dihydrogen phosphate (NaH_2PO_4, AR), hydrochloric acid (HCl, AR), aniline (AR), and hydrogen peroxide (H_2O_2, AR) were all purchased from Sinopharm Chemical Reagent Co., Ltd., China. All other chemical reagents were of analytical grade. Ultrapure water (18.25 MΩ cm) was used throughout the experiments. [C_4mim][AOT] (its chemical structure is shown in Scheme S1) was prepared according to the literature,[43,44] and its high purity was confirmed in our previous work by ^{1}H NMR spectrum and mass spectrum.[43]

Phase Diagram Construction. The T−γ fishlike phase diagram was drawn using a routine procedure which has been described in our previous work.[43,44,58] The parameters used to describe the composition of a pseudoternary HIL/buffer/surfactant (alcohol) system are defined as follows:

The mass fraction of the HIL in the mixture of the HIL and buffer (α) is given by

$$\alpha = \frac{m_{HIL}}{m_{HIL} + m_{buffer}}$$

The mass fraction of the alcohol in the surfactant mixture (δ) is given by

$$\delta = \frac{m_{alcohol}}{m_{surfactant} + m_{alcohol}}$$

The mass fraction of the surfactant (with alcohol) in the total mixture (γ) is given by

$$\gamma = \frac{m_{surfactant} + m_{alcohol}}{m_{surfactant} + m_{alcohol} + m_{HIL} + m_{buffer}}$$

For a given binary mixture of buffer (NaH_2PO_4, pH 4.3, 50 mM) and [C_8mim][PF_6] (α was set), a known amount of the surfactant [C_4mim][AOT] (with n-butanol, δ = 0.100) was added (weighed using a balance with an accuracy of ±0.1 mg). After vortexing, the resulting mixture was put in a temperature-controlled water bath (with an accuracy of ±0.1 °C) for a period of time, and the number of coexisting phases was visually determined after thermal equilibrium. For a given system, the phase inversion of the system was determined based on the change of the phase number of the system with the temperature (the temperature was adjusted in steps of 1 °C). For a given α, γ was varied by diluting the original system with the known amounts of [C_8mim][PF_6] and buffer, and then the above steps were repeated to observe the phase behavior of the system at different surfactant contents. Based on the temperature-dependent phase number of systems at different γ values, the T−γ fishlike phase diagram of the system could be plotted.

SAXS Measurement. SAXS experiments were carried out on SAXSess mc2 SAXS instrument (Anton Paar, Austria). The sample in a quartz capillary (1 mm in diameter) was first placed in the sample chamber for thermal equilibration (temperature was controlled by Anton-Paar TCS 120), then irradiated with X-ray (Cu Kα, λ = 0.154 nm) for 20 min. The data collected were corrected against the empty quartz capillary of the same type, followed by normalization by the scattering of pure water (the empty capillary scattering was subtracted). After correction of the incoherent scattering estimated from the signal at high scattering vector q, the curve of the absolute scattering intensity $I(q)$ versus q was finally obtained.

https://doi.org/10.1021/acsomega.1c03150
ACS Omega 2021, 6, 20699−20709

Determination of Kinetic Parameters of HRP. The kinetic parameters of HRP were determined based on the HRP-catalyzed oxidation of ABTS as substrate in the $[C_4mim][AOT]$-stabilized $[C_8mim][PF_6]$-based bicontinuous microemulsion. For a given α, known amounts of buffer, $[C_8mim][PF_6]$, and $[C_4mim][AOT]$ (with *n*-butanol, δ = 0.100) were mixed and equilibrated at a temperature for a period of time. After that, an aliquot of ABTS stock solution (100 mM, prepared with the buffer) and an aliquot of H_2O_2 stock solution (421.2 mM, prepared with pure water) were added and mixed well. The enzymatic reaction was initiated by adding an aliquot of HRP stock solution (0.4 μM, prepared with pure water). The reaction solution was quickly transferred to a quartz cuvette (1 cm path length), and the cuvette was set in the thermostated chamber of a UV-2550 UV−vis spectrophotometer (Shimadzu Co., Suzhou, China) to monitor the reaction by recording the time-dependent absorbance change at 420 nm. The activity of HRP at different levels of ABTS was determined based on the slope of the initial linear portion of the kinetic curve. The kinetic parameters of the HRP-catalyzed oxidation of ABTS were obtained by Lineweaver−Burk plots. The molar extinction coefficient (ε = 36,000 L mol^{-1} cm^{-1}) of the oxidation products of ABTS was considered not to vary with the composition of the microemulsion (the molecular weight of HRP is ca. 44 kDa).

Determination of the Stability of HRP. A mixed solution containing known amounts of $[C_8mim][PF_6]$, buffer, and $[C_4mim][AOT]$ (δ = 0.100) (α and γ were fixed) was placed in a thermostated water bath for thermal equilibration, and then a known volume of HRP stock solution (0.4 μM, prepared with pure water) was added and mixed quickly. The mixture was incubated at a constant temperature for a given time (t = 0, 30, 60, 90, or 120 s), and then a known volume of ABTS stock solution (100 mM, prepared with the buffer) was added. After quick mixing, an aliquot of H_2O_2 stock solution (421.2 mM, prepared with pure water) was added to initiate the enzymatic reaction. The time-dependent absorbance change at 420 nm was monitored at 20 °C on a UV-2550 UV−vis spectrophotometer (Shimadzu Co., Suzhou, China). The activity of HRP at t = 0 s was set as a reference (100%); the relative residual activity of HRP at different incubation times was then obtained. The overall initial concentrations of components in the microemulsion medium were $[ABTS]_{overall}$ = 3.0 mM, $[H_2O_2]_{overall}$ = 2.0 mM, and $[HRP]_{overall}$ = 0.0025 μM.

HRP-Catalyzed Polymerization of Aniline. Based on the selected α and γ values, a mixed solution of buffer, $[C_8mim][PF_6]$, and $[C_4mim][AOT]$ (δ = 0.100) was prepared and set in a thermostated water bath for equilibration, an aliquot of aniline stock solution (150.3 mM in 50 mM NaH_2PO_4 solution, pH adjusted to 4.3 with HCl) and an aliquot of H_2O_2 stock solution (421.2 mM, prepared with pure water) were added and mixed well, followed by adding an aliquot of HRP stock solution (896.0 μM, prepared with pure water) to trigger the reaction. The reaction system was kept in a thermostatic water bath for 12 h to complete the polymerization. The overall initial concentrations of components in the microemulsion medium were $[aniline]_{overall}$ = 8.0 mM, $[H_2O_2]_{overall}$ = 9.0 mM, and $[HRP]_{overall}$ = 2.0 μM, respectively.

UV−Vis−NIR Measurement. The UV−vis−NIR spectra of samples were recorded at room temperature on a Cary 5000 UV−vis−NIR spectrophotometer (Agilent, USA) over 350−1300 nm using the corresponding microemulsion as control. The path length was 1 cm, the scan speed was 600 nm min^{-1}, and the slit width was 2 nm.

ESR Measurement. ESR measurements were performed on a JES-X320 ESR spectrometer (Jeol, Japan). The X-band microwave frequency and the modulation frequency were 9.414 GHz and 100 kHz, respectively. The sample collected after 12 h reaction was transferred to a glass capillary (with an inner diameter of 0.9−1.1 mm) for measurement. The number of signal acquisitions was 16. DPPH was used as a standard sample; the spin concentration of a sample was calculated based on the ratio of the ESR integrated area of the sample to that of DPPH.

■ ASSOCIATED CONTENT

Supporting Information

The Supporting Information is available free of charge at https://pubs.acs.org/doi/10.1021/acsomega.1c03150.

Kinetic data for the HRP-catalyzed oxidation of ABTS in the bicontinuous microemulsion systems at different α values and at different γ values and the chemical structure of $[C_4mim][AOT]$ (PDF)

■ AUTHOR INFORMATION

Corresponding Author

Xirong Huang − *Key Laboratory of Colloid and Interface Chemistry of Ministry of Education, Shandong University, Jinan 250100, China;* orcid.org/0000-0002-7531-6283; Email: xrhuang@sdu.edu.cn

Author

Rongrong Wang − *Key Laboratory of Colloid and Interface Chemistry of Ministry of Education, Shandong University, Jinan 250100, China*

Complete contact information is available at: https://pubs.acs.org/10.1021/acsomega.1c03150

Notes

The authors declare no competing financial interest.

■ ACKNOWLEDGMENTS

We are grateful for the financial support from the National Natural Science Foundation of China (21773143, 22072074) and the Key Research and Development Plan of Shandong Province (2019GSF107090).

■ REFERENCES

(1) Wang, X.-X.; Yu, G.-F.; Zhang, J.; Yu, M.; Ramakrishna, S.; Long, Y.-Z. Conductive Polymer Ultrafine Fibers Via Electrospinning: Preparation, Physical Properties and Applications. *Prog. Mater. Sci.* **2021**, *115*, 100704.

(2) Parashar, K.; Prajapati, D.; McIntyre, R.; Kandasubramanian, B. Advancements in Biological Neural Interfaces Using Conducting Polymers: A Review. *Ind. Eng. Chem. Res.* **2020**, *59*, 9707−9718.

(3) Lee, S.; Ozlu, B.; Eom, T.; Martin, D. C.; Shim, B. S. Electrically Conducting Polymers for Bio-Interfacing Electronics: From Neural and Cardiac Interfaces to Bone and Artificial Tissue Biomaterials. *Biosens. Bioelectron.* **2020**, *170*, 112620.

(4) Shoaie, N.; Daneshpour, M.; Azimzadeh, M.; Mahshid, S.; Khoshfetrat, S. M.; Jahanpeyma, F.; Gholaminejad, A.; Omidfar, K.; Foruzandeh, M. Electrochemical Sensors and Biosensors Based on the Use of Polyaniline and Its Nanocomposites: A Review on Recent Advances. *Microchim. Acta* **2019**, *186*, 465.

(5) Baker, C. O.; Huang, X.; Nelson, W.; Kaner, R. B. Polyaniline Nanofibers: Broadening Applications for Conducting Polymers. *Chem. Soc. Rev.* **2017**, *46*, 1510−1525.
(6) Zhou, Q.; Wang, J.; Ma, Y.; Cong, C.; Wang, F. The Relationship of Conductivity to the Morphology and Crystallinity of Polyaniline Controlled by Water Content Via Reverse Microemulsion. *Colloid Polym. Sci.* **2007**, *285*, 405−411.
(7) Shen, L.; Huang, X. Electrochemical Polymerization of Aniline in a Protic Ionic Liquid with High Proton Activity. *Synth. Met.* **2018**, *245*, 18−23.
(8) Shen, L.; Gao, N.; Huang, X. Synthesis, Characterization and Electropolymerization of Functionalized Organic Salt−Anilinium Saccharinate and Electrochemically Controlled Release of Saccharinate Anions. *Electrochim. Acta* **2020**, *329*, 135142.
(9) Kobayashi, S.; Makino, A. Enzymatic Polymer Synthesis: An Opportunity for Green Polymer Chemistry. *Chem. Rev.* **2009**, *109*, 5288−5353.
(10) Kim, S.-C.; Huh, P.; Kumar, J.; Kim, B.; Lee, J.-O.; Bruno, F. F.; Samuelson, L. A. Synthesis of Polyaniline Derivatives Via Biocatalysis. *Green Chem.* **2007**, *9*, 44−48.
(11) Ćirić-Marjanović, G.; Milojević-Rakić, M.; Janošević-Ležaić, A.; Luginbühl, S.; Walde, P. Enzymatic Oligomerization and Polymerization of Arylamines: State of the Art and Perspectives. *Chem. Pap.* **2017**, *71*, 199−242.
(12) Itoh, T.; Takagi, Y. Laccase-Catalyzed Reactions in Ionic Liquids for Green Sustainable Chemistry. *ACS Sustainable Chem. Eng.* **2021**, *9*, 1443−1458.
(13) Walde, P.; Guo, Z. Enzyme-Catalyzed Chemical Structure-Controlling Template Polymerization. *Soft Matter* **2011**, *7*, 316−331.
(14) Leppänen, A.-S.; Xu, C.; Liu, J.; Wang, X.; Pesonen, M.; Willför, S. Anionic Polysaccharides as Templates for the Synthesis of Conducting Polyaniline and as Structural Matrix for Conducting Biocomposites. *Macromol. Rapid Commun.* **2013**, *34*, 1056−1061.
(15) Fujisaki, T.; Kashima, K.; Serrano-Luginbühl, S.; Kissner, R.; Bajuk-Bogdanović, D.; Milojević-Rakić, M.; Ćirić-Marjanović, G.; Busato, S.; Lizundia, E.; Walde, P. Effect of Template Type on the Preparation of the Emeraldine Salt Form of Polyaniline (PANI-ES) with Horseradish Peroxidase Isoenzyme C (HRPC) and Hydrogen Peroxide. *RSC Adv.* **2019**, *9*, 33080−33095.
(16) Zhang, J.; Zou, F.; Yu, X.; Huang, X.; Qu, Y. Ionic Liquid Improves the Laccase-Catalyzed Synthesis of Water-Soluble Conducting Polyaniline. *Colloid Polym. Sci.* **2014**, *292*, 2549−2554.
(17) Giacobbe, S.; Pezzella, C.; Della Ventura, B.; Giacobelli, V. G.; Rossi, M.; Fontanarosa, C.; Amoresano, A.; Sannia, G.; Velotta, R.; Piscitelli, A. Green Synthesis of Conductive Polyaniline by Trametes Versicolor Laccase Using a DNA Template. *Eng. Life Sci.* **2019**, *19*, 631−642.
(18) Liu, W.; Cholli, A. L.; Nagarajan, R.; Kumar, J.; Tripathy, S.; Bruno, F. F.; Samuelson, L. The Role of Template in the Enzymatic Synthesis of Conducting Polyaniline. *J. Am. Chem. Soc.* **1999**, *121*, 11345−11355.
(19) Küchler, A.; Yoshimoto, M.; Luginbühl, S.; Mavelli, F.; Walde, P. Enzymatic Reactions in Confined Environments. *Nat. Nanotechnol.* **2016**, *11*, 409−420.
(20) Liu, W.; Kumar, J.; Tripathy, S.; Samuelson, L. A. Enzymatic Synthesis of Conducting Polyaniline in Micelle Solutions. *Langmuir* **2002**, *18*, 9696−9704.
(21) Zou, F.; Xue, L.; Yu, X.; Li, Y.; Zhao, Y.; Lu, L.; Huang, X.; Qu, Y. One Step Biosynthesis of Chiral, Conducting and Water Soluble Polyaniline in AOT Micellar Solution. *Colloids Surf., A* **2013**, *429*, 38−43.
(22) Zou, F.; Li, Y.; Yu, X.; Zhang, J.; Huang, X.; Qu, Y. β-Cyclodextrin Improves the Linearity of Polyaniline Synthesized Enzymatically in AOT Micellar Solution. *J. Mol. Catal. B: Enzym.* **2014**, *104*, 35−41.
(23) Caramyshev, A. V.; Lobachov, V. M.; Selivanov, D. V.; Sheval, E. V.; Vorobiev, A. K.; Katasova, O. N.; Polyakov, V. Y.; Makarov, A. A.; Sakharov, I. Y. Micellar Peroxidase-Catalyzed Synthesis of Chiral Polyaniline. *Biomacromolecules* **2007**, *8*, 2549−2555.
(24) Hu, X.; Shu, X.-S.; Li, X.-W.; Liu, S.-G.; Zhang, Y.-Y.; Zou, G.-L. Hemoglobin-Biocatalyzed Synthesis of Conducting Polyaniline in Micellar Solutions. *Enzyme Microb. Technol.* **2006**, *38*, 675−682.
(25) Guo, H.; Chen, J.; Xu, Y. Hb-Induced Biocatalyzed Synthesis of Water-Soluble Polyaniline Nanocomposites with Controlled Handedness in DBSA−CTAB Mixed Micelle Solutions. *Synth. Met.* **2015**, *205*, 169−174.
(26) Luginbühl, S.; Bertschi, L.; Willeke, M.; Schuler, L. D.; Walde, P. How Anionic Vesicles Steer the Oligomerization of Enzymatically Oxidized p-Aminodiphenylamine (PADPA) toward a Polyaniline Emeraldine Salt (PANI-ES)-Type Product. *Langmuir* **2016**, *32*, 9765−9779.
(27) Zhang, Y.; Serrano-Luginbühl, S.; Kissner, R.; Milojević-Rakić, M.; Bajuk-Bogdanović, D.; Ćirić-Marjanović, G.; Wang, Q.; Walde, P. Enzymatic Synthesis of Highly Electroactive Oligoanilines from a p-Aminodiphenylamine/Aniline Mixture with Anionic Vesicles as Templates. *Langmuir* **2018**, *34*, 9153−9166.
(28) Junker, K.; Zandomeneghi, G.; Guo, Z.; Kissner, R.; Ishikawa, T.; Kohlbrecher, J.; Walde, P. Mechanistic Aspects of the Horseradish Peroxidase-Catalysed Polymerisation of Aniline in the Presence of AOT Vesicles as Templates. *RSC Adv.* **2012**, *2*, 6478−6495.
(29) Guo, Z.; Hauser, N.; Moreno, A.; Ishikawa, T.; Walde, P. AOT Vesicles as Templates for the Horseradish Peroxidase-Triggered Polymerization of Aniline. *Soft Matter* **2011**, *7*, 180−193.
(30) Chen, J.; Bai, L.; Yang, M.; Guo, H.; Xu, Y. Biocatalyzed Synthesis of Conducting Polyaniline in Reverse Microemulsions. *Synth. Met.* **2014**, *187*, 108−112.
(31) Kahlweit, M.; Strey, R.; Busse, G. Microemulsions: A Qualitative Thermodynamic Approach. *J. Phys. Chem.* **1990**, *94*, 3881−3894.
(32) Kahlweit, M.; Strey, R.; Haase, D.; Kunieda, H.; Schmeling, T.; Faulhaber, B.; Borkovec, M.; Eicke, H. F.; Busse, G.; Eggers, F.; Funck, T.; Richmann, H.; Magid, L.; Söderman, O.; Stilbs, P.; Winkler, J.; Dittrich, A.; Jahn, W. How to Study Microemulsions. *J. Colloid Interface Sci.* **1987**, *118*, 436−453.
(33) Schneider, K.; Ott, T. M.; Schweins, R.; Frielinghaus, H.; Lade, O.; Sottmann, T. Phase Behavior and Microstructure of Symmetric Nonionic Microemulsions with Long-Chain *n*-Alkanes and Waxes. *Ind. Eng. Chem. Res.* **2019**, *58*, 2583−2595.
(34) Gradzielski, M.; Duvail, M.; de Molina, P. M.; Simon, M.; Talmon, Y.; Zemb, T. Using Microemulsions: Formulation Based on Knowledge of Their Mesostructure. *Chem. Rev.* **2021**, *121*, 5671−5740.
(35) Jin, W.; Wang, R.; Huang, X. Horseradish Peroxidase-Catalyzed Oxidative Polymerization of Aniline in Bicontinuous Microemulsion Stabilized by AOT/SDS. *J. Mol. Liq.* **2020**, *302*, 112529.
(36) Jin, W.; Wang, R.; Huang, X. Improvement of Enzymatic Synthesis of Conducting Polyaniline in Anionic Surfactant AOT Stabilized Bicontinuous Microemulsion by Adding Zwitterionic Surfactant SB-12. *J. Mol. Liq.* **2020**, *312*, 113442.
(37) Rogers, R. D.; Seddon, K. R. Ionic Liquids: Solvents of the Future? *Science* **2003**, *302*, 792−793.
(38) Porada, J. H.; Zauser, D.; Feucht, B.; Stubenrauch, C. Tailored Ionic Liquid-Based Surfactants for the Formation of Microemulsions with Water and a Hydrophobic Ionic Liquid. *Soft Matter* **2016**, *12*, 6352−6356.
(39) Yu, X.; Li, Q.; Wang, M.; Du, N.; Huang, X. Study on the Catalytic Performance of Laccase in the Hydrophobic Ionic Liquid-Based Bicontinuous Microemulsion Stabilized by Polyoxyethylene-Type Nonionic Surfactants. *Soft Matter* **2016**, *12*, 1713−1720.
(40) Porada, J. H.; Mansueto, M.; Laschat, S.; Stubenrauch, C. Microemulsions with Hydrophobic Ionic Liquids: Influence of the Structure of the Anion. *J. Mol. Liq.* **2017**, *227*, 202−209.
(41) Hejazifar, M.; Lanaridi, O.; Bica-Schröder, K. Ionic Liquid Based Microemulsions: A Review. *J. Mol. Liq.* **2020**, *303*, 112264.
(42) Gao, Y.; Li, N.; Zheng, L.; Zhao, X.; Zhang, S.; Han, B.; Hou, W.; Li, G. A Cyclic Voltammetric Technique for the Detection of Micro-Regions of $BmimPF_6$/Tween 20/H_2O Microemulsions and

https://doi.org/10.1021/acsomega.1c03150
ACS Omega 2021, 6, 20699−20709

Their Performance Characterization by UV-Vis Spectroscopy. *Green Chem.* **2006**, *8*, 43−49.
(43) Wang, R.; Feng, Z.; Jin, W.; Huang, X. Phase Behavior of the Anionic Surfactant [Bmim][AOT]-Stabilized Hydrophobic Ionic Liquid-Based Microemulsions and the Effect of *n*-Alcohols. *Ind. Eng. Chem. Res.* **2018**, *57*, 14846−14853.
(44) Wang, R.; Huang, X. Anionic Surfactant-Stabilized Hydrophobic Ionic Liquid-Based Bicontinuous Microemulsion: Formulation, Microstructure and Laccase Kinetics. *J. Mol. Liq.* **2019**, *292*, 111404.
(45) Zhang, Y.; Zhang, X. Y.; Chai, J. L.; Cui, X. C.; Pan, J.; Song, J. W.; Sun, B.; Lu, J. J. The Phase Behavior and Solubilization of Isopropyl Myristate in Microemulsions Containing Hexadecyl Trimethyl Ammonium Bromide and Sodium Dodecyl Sulfate. *J. Mol. Liq.* **2017**, *244*, 262−268.
(46) Burauer, S.; Sachert, T.; Sottmann, T.; Strey, R. On Microemulsion Phase Behavior and the Monomeric Solubility of Surfactant. *Phys. Chem. Chem. Phys.* **1999**, *1*, 4299−4306.
(47) Kahlweit, M.; Strey, R.; Schomaecker, R.; Haase, D. General Patterns of the Phase Behavior of Mixtures of Water, Nonpolar Solvents, Amphiphiles, and Electrolytes. *Langmuir* **1989**, *5*, 305−315.
(48) Dmitrieva, E.; Dunsch, L. How Linear Is "Linear" Polyaniline? *J. Phys. Chem. B* **2011**, *115*, 6401−6411.
(49) Luginbühl, S.; Milojević-Rakić, M.; Junker, K.; Bajuk-Bogdanović, D.; Pašti, I.; Kissner, R.; Ćirić-Marjanović, G.; Walde, P. The Influence of Anionic Vesicles on the Oligomerization of p-Aminodiphenylamine Catalyzed by Horseradish Peroxidase and Hydrogen Peroxide. *Synth. Met.* **2017**, *226*, 89−103.
(50) Hashimoto, K.; Fujii, K.; Kusano, T.; Hirosawa, K.; Shibayama, M. Small-Angle X-Ray Scattering Study on Nano-Scale Structures Controlled by Water Content in a Binary Water/Ionic Liquid System. *Phys. Chem. Chem. Phys.* **2018**, *20*, 18355−18360.
(51) Greaves, T. L.; Drummond, C. J. Solvent Nanostructure, the Solvophobic Effect and Amphiphile Self-Assembly in Ionic Liquids. *Chem. Soc. Rev.* **2013**, *42*, 1096−1120.
(52) Thater, J. C.; Stubenrauch, C.; Glatter, O.; Klemmer, H.; Sottmann, T. Microstructure of Ionic Liquid (EAN)-Rich and Oil-Rich Microemulsions Studied by SANS. *Phys. Chem. Chem. Phys.* **2019**, *21*, 160−170.
(53) Teubner, M.; Strey, R. Origin of the Scattering Peak in Microemulsions. *J. Chem. Phys.* **1987**, *87*, 3195−3200.
(54) Hayes, D. G.; Gomez del Rio, J. A.; Ye, R.; Urban, V. S.; Pingali, S. V.; O'Neill, H. M. Effect of Protein Incorporation on the Nanostructure of the Bicontinuous Microemulsion Phase of Winsor-III Systems: A Small-Angle Neutron Scattering Study. *Langmuir* **2015**, *31*, 1901−1910.
(55) Anjum, N.; Guedeau-Boudeville, M.-A.; Stubenrauch, C.; Mourchid, A. Phase Behavior and Microstructure of Microemulsions Containing the Hydrophobic Ionic Liquid 1-Butyl-3-Methylimidazolium Hexafluorophosphate. *J. Phys. Chem. B* **2009**, *113*, 239−244.
(56) Atkin, R.; Warr, G. G. Phase Behavior and Microstructure of Microemulsions with a Room-Temperature Ionic Liquid as the Polar Phase. *J. Phys. Chem. B* **2007**, *111*, 9309−9316.
(57) Mitsou, E.; Kalogianni, E. P.; Georgiou, D.; Stamatis, H.; Xenakis, A.; Zoumpanioti, M. Formulation and Structural Study of a Biocompatible Water-in-Oil Microemulsion as an Appropriate Enzyme Carrier: The Model Case of Horseradish Peroxidase. *Langmuir* **2019**, *35*, 150−160.
(58) Wang, R.; Jin, W.; Huang, X. Construction of Zwitterionic Surfactant-Stabilized Hydrophobic Ionic Liquid-Based Bicontinuous Microemulsion and Microstructure-Dependent Activity of Solubilized Lipase. *J. Mol. Liq.* **2020**, *317*, 114011.
(59) Stejskal, J.; Riede, A.; Hlavatá, D.; Prokeš, J.; Helmstedt, M.; Holler, P. The Effect of Polymerization Temperature on Molecular Weight, Crystallinity, and Electrical Conductivity of Polyaniline. *Synth. Met.* **1998**, *96*, 55−61.
(60) Adams, P. N.; Laughlin, P. J.; Monkman, A. P.; Kenwright, A. M. Low Temperature Synthesis of High Molecular Weight Polyaniline. *Polymer* **1996**, *37*, 3411−3417.

https://doi.org/10.1021/acsomega.1c03150
ACS Omega 2021, 6, 20699−20709